J Nanopart Res (2012) 14:1299
DOI 10.1007/s11051-012-1299-1

BRIEF COMMUNICATION

One-step synthesis of bioactive glass by spray pyrolysis

Shao-Ju Shih · Yu-Jen Chou · I-Chen Chien

Received: 21 May 2012 / Accepted: 9 November 2012 / Published online: 24 November 2012

Abstract Bioactive glasses (BGs) have recently received more attention from biologists and engineers because of their potential applications in bone implants. The sol–gel process is one of the most popular methods for fabricating BGs, and has been used to produce BGs for years. However, the sol–gel process has the disadvantages of discontinuous processing and a long processing time. This study presented a one-step spray pyrolysis (SP) synthesis method to overcome these disadvantages. This SP method has synthesized spherical bioactive glass (SBG) and mesoporous bioactive glass (MBG) particles using Si-, Ca- and P-based precursors. This study used transmission electron microscopy, selected area electron diffraction and X-ray dispersive spectroscopy to characterize the microstructure, crystallographic structure, and chemical composition for the BG particles. In addition, in vitro bioactive tests showed the formation of hydroxyl apatite layers on SBG and MBG particles after immersion in simulated body fluid for 5 h. Experimental results show the SP formation mechanisms of SBG and MBG particles.

S.-J. Shih (✉) · Y.-J. Chou · I.-C. Chien
Department of Materials Science and Engineering,
National Taiwan University of Science and Technology,
43, Sec. 4 Keelung Road, Taipei 10607, Taiwan
e-mail: shao-ju.shih@mail.ntust.edu.tw

Keywords Bioactive glass · Mesoporous · Spray pyrolysis · In vitro bioactivity · Electron microscopy

Introduction

Bioactive glasses (BGs) have attracted considerable attention since they were first reported by Hench et al. in 1971. The common compositions of BGs are SiO_2, CaO, and P_2O_5 (Li et al. 1991; Hench and Polak 2002). Early studies demonstrated that when these BGs are implanted in the human body, the surfaces of the BGs form hydroxyl apatite (HA) layers, which constitute the main inorganic components of humans (Li et al. 1991; Xia and Chang 2008). These HA layers chemically bond with human bones (Vallet-Regi 2001). Thus, BGs have become one of the most popular materials for bone implants.

Previous studies have applied conventional glass processes to prepare BGs (Vogel and Höland 1982; Vogel et al. 1986). For example, the 45S5 BG® (Copyrights, University of Florida, Gainesville, FL 32611) is the first and the most popular bioactive glass available. After Li et al. (1991) successfully used the sol–gel process for BG fabrication in 1991, the sol–gel process has become a popular alternative method for BG synthesis because of the following advantages. First, the sol–gel process offers a lower heat treatment temperature (600–700 °C) than that (1,250–1,400 °C) of the conventional glass process,

which offers an advantage of a lower cost. Second, the conventional glass process, which involves grinding and sieving procedures (causing contaminants) has difficulty fabricating high purity glasses for bioactive control. Third, the sol–gel process provides a broader range and greater control of bioactivity because it can alter the BG composition or microstructure by manipulating processing parameters (Hench 1997). For example, Xia and Chang used the sol–gel process to mix the tri-block surfactants of P123 ($EO_{20}PO_{70}EO_{20}$, where EO is poly ethylene oxide and PO is poly propylene oxide) with the SiO_2–CaO–P_2O_5 precursors for preparing the well-ordered mesoporous bioactive glasses (MBGs) (Xia and Chang 2006). These MBGs were able to enhance HA formation than conventional glasses (Xia and Chang 2006). Although the sol–gel process has been used for BG fabrication, it has the disadvantages of discontinuous processing (unsuitable for mass production) and a long processing time ($\sim$1–2 days) (Shih et al. 2010). On the other hand, the spray pyrolysis (SP) method has the advantages of continuous processing and a shorter process time ($\sim$1 h) (Shih et al. 2009). SP method has been used to produce various nanoparticles (Chen et al. 2007), and recently SP method has also been applied to prepare borate-based BG submicron particles (Cho and Kang 2009) and 45S5 BG nanoparticles (Mačković et al. 2012). For example, Mačković et al. prepared 45S5 BG nanoparticles using a flame spray synthesis. Due to their high surface area, these nanoparticles preformed rapid formation of HA after 1 day of immersion in simulated body fluid (SBF) compared to 3 days for the similar micron-sized particles (Mačković et al. 2012). So far only a few studies have focused on preparing mesoporous structures using SP. Therefore, developing the SP method is essential for MBG fabrication.

The SP process involves four main stages, including: atomization, solvent evaporation, solute decomposition, and particle sintering to transform liquid precursors to solid particles. Initially the precursor solution is atomized into droplets using an ultrasonic nebulizer. These droplets then flow through a furnace and undergo solvent evaporation (drying). Meanwhile, the solutes in these dried droplets start precipitation and decomposition to form particles. Finally, sintering of these particles forms various structures (e.g., solid, hollow, or porous). Further details of these four stages can be found in Ref. (Messing et al. 1993).

Many SP parameters for morphology and particle size control have been investigated (Messing et al. 1993; Shih et al. 2011; Shih et al. 2012). Particle morphology is mainly determined by precursor solubilities, melting temperatures, and evaporation behaviors. High precursor solubilities undergo the volume precipitation mechanism to form solid structures, whereas low precursor solubilities undergo the surface precipitation mechanism to form hollow structures (Messing et al. 1993). When the precursor melting temperature is lower than water evaporation temperature, the molten precursors inhibit the removal of the entrapped water to form porous structures (Shih et al. 2012). Solvent evaporation behaviors also play a role in the morphology control. For example, for the precursors with low solubilities, the solutes of the larger droplets precipitate faster on the surface than in the center to form solid shells (hollow particles), whereas the solutes of the smaller droplets precipitate simultaneously in all volume to form solid particles due to a short evaporation path (Shih et al. 2012).

This study reports the preparation and analysis of spherical bioactive glass (SBG) and MBG particles. The morphologies and the particle size distribution of these materials were characterized using transmission electron microscopy (TEM) (Tecnai G2 F20, FEI, USA). Selected area electron diffraction (SAED) patterns were used to check the crystallinity of particles. The number of pores in the MBG particles was measured from a number of TEM micrographs, which revealed more than 100 pores. The surface area of these particles was determined using the nitrogen adsorption method (Brunauer et al. 1938) [the Brunauer–Emmett–Teller (BET) method] (Tristar, Micromeritics, US) and compared with the observed morphologies. In addition, X-ray energy-dispersive spectroscopy (XEDS) was conducted to examine the chemical compositions of the particles. For the in vitro bioactive test, X-ray diffraction (XRD) (D2 Phaser, Bruker) technique was used to characterize BG particles before and after immersing in the SBF, which has an ion concentration nearly equal to that of the human blood plasma (KuKubo et al. 1990). Based on the combined experimental results of TEM and BET, this study proposes a formation mechanism of SBG and MBG particles.

Experimental

Synthesis

The SBG and the MBG particles were prepared by SP in this study. In order to give a comparative study of the SP particles with the sol–gel particles, the same composition with the previous MBG particles prepared by the sol–gel method (Shih et al. 2010) has been used. The precursors of the solid particles were 6.7 g tetraethyl orthosilicate [TEOS, $Si(OC_2H_5)_4$, 99.9 wt%, Showa, Japan], 1.4 g calcium nitrate tetrahydrate (CN, $Ca(NO_3)_2{\cdot}4H_2O$, 98.5 wt%, Showa, Japan), and 0.73 g triethyl phosphate (TEP, $(C_2H_5)_3PO_4$, 99 wt%, Alfa Aesar, US) (the molar ratio of Si:Ca:P = 76:14:10). Also, the precursors of mesoporous particles were 6.7 g TEOS, 1.4 g CN, 0.73 g TEP, and 7.0 g tri-block surfactant (Pluronic F-127, Sigma-Aldrich, Germany) (F127, $EO_{106}PO_{70}EO_{106}$). The precursors of the solid and mesoporous particles were dissolved in 1.0 g 0.5 M HCl and 60.0 g ethanol and stirred at room temperature for 24 h. For SP, the solution (the mixture of the 10 ml precursor solution and 390 ml DI-water) was dispersed into fine droplets with the frequency of 1.65 MHz. Subsequently, these droplets in the reactor, with three different heating zones of 250, 700, and 350 °C, undergo solvent evaporation, solute precipitation, and precursor decomposition to convert into bioactive glass particles. The surface of the particles was charged by electron released from the tungsten corona wire at high voltage (16 kV). Finally, the

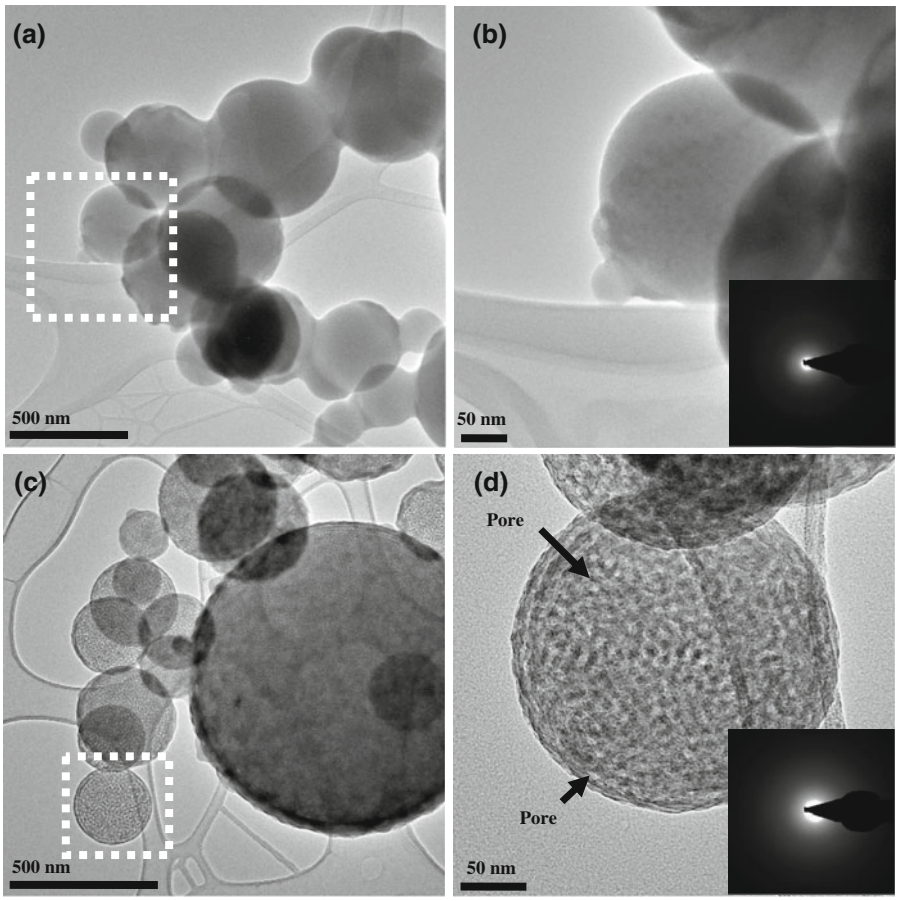

Fig. 1 The TEM images of the typical SBG and MBG particles. **a** A cluster of SBG particles with diameters in the ~50–470 nm range and **b** the enlarge image of the SBG particles, as the *dashed square* in (**a**). **c** A cluster of MBG particles with diameters in the ~35–1,050 nm range and **d** the enlarged image of the MBG particles, as the *dashed square* in (**c**). The SAED patterns of the SBG and MBG particles in (**b**) and in (**d**) are shown as *insets* in the corresponding images

negative charged powder was neutralized and condensed in an earthed stainless steel collector.

Morphology characterization

To prepare the particles for the morphology observation, the particles were first dispersed in acetone in an ultrasonic bath for 5 min, and then a drop of suspension was placed onto a carbon film grid. Then the solvent on the carbon grid was evaporated at room temperature. The field emission gun TEM (Tecnai G2 F20, FEI, USA), operated at 200 keV, was carried out to characterize the morphology and the particle diameter distribution. In addition, the SAED patterns were recorded to examine the phase state of the material. In addition, XEDS with a probe size of $\sim$500 nm containing several particles was employed to determine chemical compositions. The specific surface area data of the particles were determined by the BET method from nitrogen adsorption and desorption isotherm data obtained at -196 °C on a constant-volume adsorption apparatus. The as-prepared samples were degassed at 150 °C for 3 h before measurements.

In vitro bioactive test

The in vitro bioactivity tests for the particles of SBG and MBG were carried out using the SBF. The ion concentrations of SBF are Na^+ 142.0, K^+ 5.0, Mg^{2+} 1.5, Ca^{2+} 2.5, Cl^- 147.8, HCO_3^- 4.2, HPO_4^{2-} 1.0, and SO_4^{2-} 0.5 mmol L^{-1} (mM). The bioactivity was tested by immersing the particles in SBF at a solid:liquid ratio of 1 g: 10 ml at 37 °C for 0.5 h. X-ray diffractometer (D2 Phaser, Bruker, German), with Ni-filtered Cu Kα radiation, was used to characterize the surfaces of the SBG and the MBG particles before and after immersing in SBF.

Results and discussion

Morphology and crystallographic structure

Figure 1 shows the TEM micrographs and the SAED patterns of typical SBG and MBG particles. Figure 1a, c indicate that the SBG particles (diameter range of $\sim$50–470 nm) and the MBG particles (diameter range of $\sim$35–1050 nm) are spherical, and not hollow or irregular. This result suggests that the SBG and MBG precursors have high solubilities in water. Therefore, the solute in the precursor droplets precipitates homogenously during the drying process to create spherical particles [i.e., volume precipitation (Messing et al. 1993)]. Figure 1b, d present the fuzzy rings in the SAED patterns, indicating that the SBG and MBG particles are amorphous. In addition, Fig. 1b, d show the morphology of the SBG and MBG particles, respectively. The SBG particles show a continuous contrast (Fig. 1b), whereas the MBG particles show discontinuous bright contrast regions (indicated as black arrows in Fig. 1d). This diffraction contrast is associated mainly with thickness and crystal orientations in TEM images. In this case, since the particles are amorphous (random orientations), the continuous and bright contrasts directly correspond to thickness (i.e., a pore region shows brighter contrast than a solid region). Thus, TEM experimental results show that the

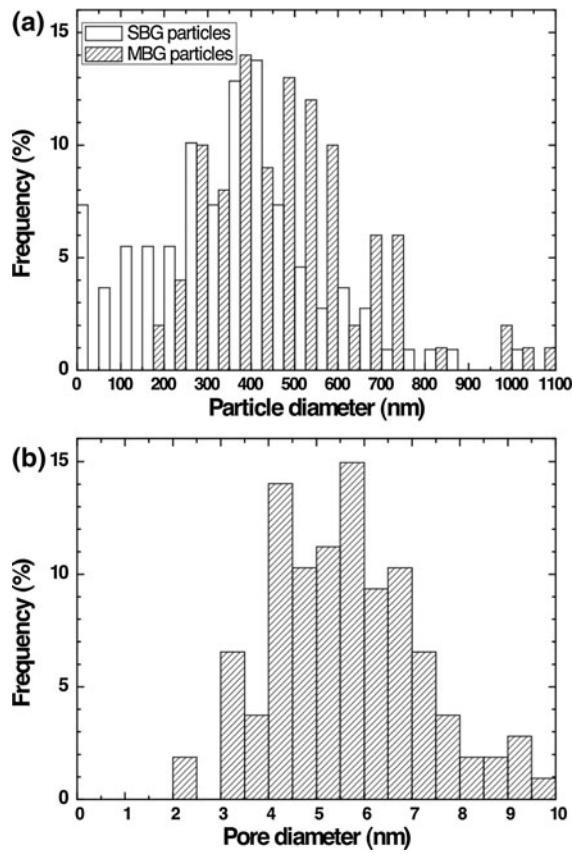

Fig. 2 The particle diameter distributions of **a** the SBG and MBG particles, and **b** the pore diameter distribution of the MBG particles

morphologies of the SBG and MBG particles are solid and porous, respectively.

Figure 2 shows the particle diameters and pore size histograms of the particles. The average diameters of the SBG and MBG particles are 383 ± 260 and 489 ± 195 nm, respectively. A range of SP conditions, including precursor properties, size distribution of droplets, and furnace temperatures affect the particle morphology. To study the influence of the precursors, the SP conditions were held constant in experiments involving various precursors. The size and distribution of droplets were mainly controlled by the precursor solution density and ultrasonic frequency of the nebulizer (Song et al. 2004); thus, the same solution concentration and frequency were applied for both samples in this study. Since SP particles are generated using a "one-particle-per-drop" mechanism, particle size is directly related to droplet size. For the SBG particles, the precursor concentration and ultrasonic frequency used are similar to Chen et al's (2008) work; therefore, the synthesized particles show similar averaged particle sizes (383 nm for SBG particles and 340 for ceria particles). Furthermore, smaller sized nanoparticles can be achieved by decreasing precursor concentration [average size of 95 nm using the precursor concentration of 0.01 wt% (Chen et al. 2008)]. For the MBG particles, since SBG and MBG have similar droplet distributions, the MBG particles may be larger than the SBG particles because of decomposition of the F-127 surfactants, which produces a void area during SP. The average pore size of the MBG particles is 5.6 ± 1.6 nm. In addition, BET data confirm that the MBG particles have a substantially larger surface area (250.1 m^2 g^{-1}) than the SBG particles (8.0 m^2g^{-1}).

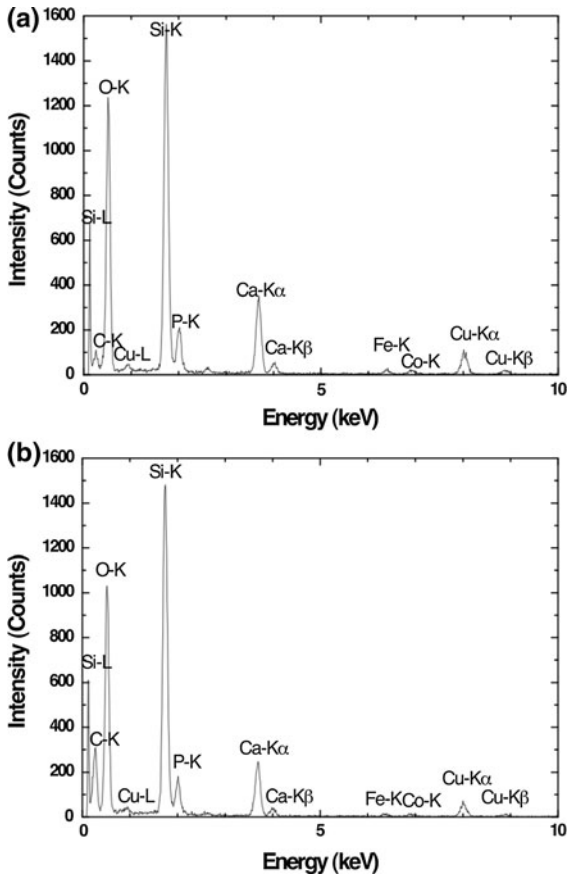

Fig. 3 The XEDS spectra for **a** the SBG and **b** MBG particles

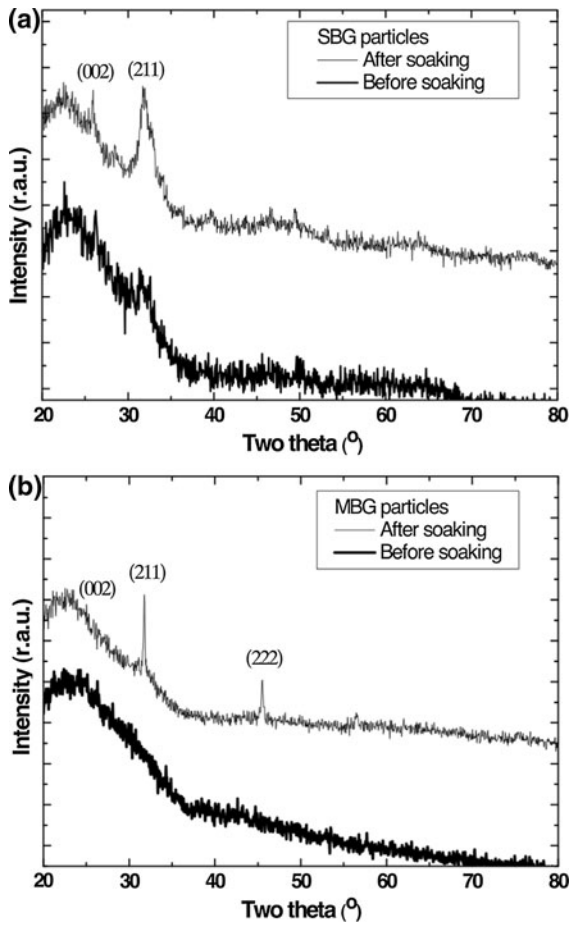

Fig. 4 The XRD patterns of **a** the SBG particles and **b** MBG particles before and after soaking in SBF solution for 0.5 h. The indexed peaks belong to the HA phase (JCPDF number of 84-1998)

Chemical composition

Figure 3a, b represent the XEDS spectra of the SBG and MBG particles after background removal, respectively. The X-ray peaks of C–K, Cu–K, and Cu–L were generated from carbon film grids. The X-ray peaks of Fe–K and Co–K were generated from the microscope aperture, which should not be considered. These XEDS results indicate that the composition of Si, Ca, and P is 74.8:15.6:9.6 (by atomic ratio) for the SBG particles and 77.7:12.8:9.5 (by atomic ratio) for the MBG particles. Thus, the XEDS data show that the compositions of the BG particles are close to the initial composition of the precursor solution (Si:Ca:P = 76:14:10 by atomic ratio), indicating an excellent composition control of the SP process.

In vitro bioactive test for bioactive glass

Figure 4 shows the XRD patterns of the SBG and MBG particles before and after immersing in SBF. The results confirm that the SBG and MBG particles are amorphous before soaking: no diffraction maximum is observed and only a broad band between 20° and 37° is apparent. After soaking in SBF for 0.5 h, two main diffraction peaks appear at 25.8° and 31.7°, corresponding to the (002) and (211) planes of HA (JCPDF number of 84-1998). Bioactivities are directly related to the crystal growth rates of HA in SBF. Figure 4 shows that soaked SBG particles have a broader (211) peak compared to that of the soaked MBG particles. Based on Scherrer's formula (Cullity and Stock 2001), we calculated that the HA crystals for the SBG particles are ~5 nm and that for the MBG particles are ~40 nm. This result shows that MBG particles have better bioactivities (faster HA formation speed) than that of the SBG particles, which suggests that higher surface area does enhance bioactivities for BGs. Furthermore, we have compared the SP derived particles with the same sol–gel derived particles (Shih et al. 2010) with the same chemical composition. With the similar surface area (250.1 m^2/g for the SP derived

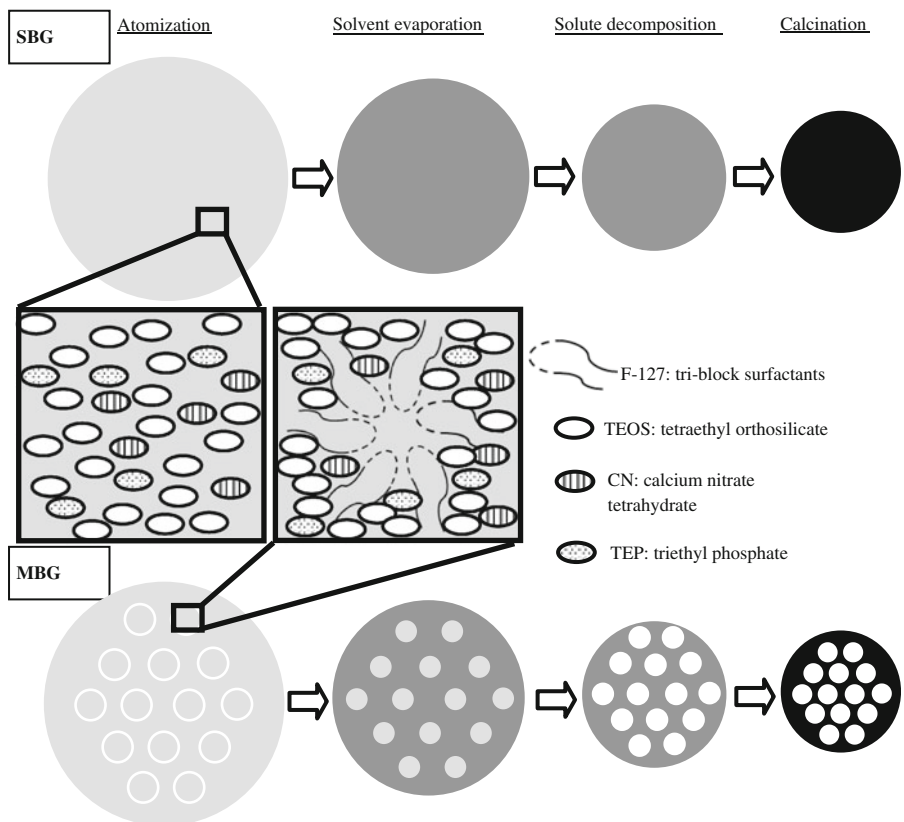

Fig. 5 The schematic diagram of the SBG and MBG particles prepared using SP

particles and 328.7 m^2/g for the sol–gel derived particles), the time required for HA formation for the SP particles (0.5 h) is much shorter than that of the sol–gel derived particles (4 h) suggesting that the SP particles have better bioactive properties than that of the sol–gel particles. Thus, the in vitro bioactive tests in this study indicate that both the SBG and MBG particles have sufficient bioactivity to form HA layers after immersion SBF. According to the experimental results of TEM, SAED, BET, XEDS, and the in vitro bioactive tests (XRD), two types of BG particles (i.e., SBG and MBG) were successfully synthesized using the SP process in this study.

Morphology formation

Figure 5 shows a schematic diagram of the formation mechanism of the SBG and MBG particles. For SBG, the TEOS, CN and TEP precursors are orientated randomly in a droplet in the atomization stage. These precursors precipitate and decompose homogenously in the droplet during the stages of solvent evaporation and solute decomposition because of the high precursor solubility, called volume precipitation (Messing et al. 1993). Subsequently, with increasing of temperature, spherical SBG particles form during the final stage of calcination. Unlike the SBG droplets, the MBG droplets have extra F-127 surfactants. These surfactants form micelles when their reach to a critical concentration in the atomization stage (Vallet-Regi et al. 2008). For these micelles, the hydrophilic PO groups gather outside, whereas the hydrophobic EO groups gather inside. The micelles aggregate themselves and form into supramicellar structures (Vallet-Regi et al. 2008), and the TEOS, CN and TEP precursors are subsequently surrounded by hydrophilic PO groups (outside of the micelles), as shown in Fig. 5. After the stages of evaporation, decomposition, and calcination, these micelles form a porous framework for the MBG particles. In summary, this study proposes SP formation mechanisms for SBG and MBG particles.

Conclusions

This study reports the synthesis of spherical SBG and MBG particles using the SP process. This study also characterizes the morphologies, crystallographic structures, and chemical compositions of the BG particles using TEM, SAED, BET, and XEDS. Compared to SBG particles, the porous structure of the MBG particles was generated by the supramicellar structures of F-127 surfactants achieving a high surface area and higher bioactivities than the solid SBG particles. The in vitro bioactive test results in this study confirm the existence of HA layers on the surfaces of the BG particles by XRD. Finally, this study proposes the formation mechanisms of BGs using SP, which are potential for more complex BG systems and are thought to be important materials for bone implants.

Acknowledgments The authors acknowledge the financial support from National Taiwan University of Science and Technology (Grant No. 100H451201) and from the National Science Council of Taiwan (Grant No. NSC 101-2628-E-011-008-MY2).

References

Brunauer S, Emmett PH, Teller E (1938) Adsorption of gases in multimolecular layers. J Am Chem Soc 60:309–319

Chen CY, Lyu YR, Su CY, Lin HM, Lin CK (2007) Characterization of spray pyrolyzed manganese oxide powders deposited by electrophoretic deposition technique. Surf Coat Technol 202:1277–1281

Chen CY, Tseng TK, Tsay CY, Lin CK (2008) Formation of irregular nanocrystalline CeO_2 particles from acetate-based precursor via spray pyrolysis. J Mater Eng Perform 17:20–24

Cho JS, Kang YC (2009) Synthesis of spherical shape borate-based bioactive glass powders prepared by ultrasonic spray pyrolysis. Ceram Int 35:2103–2109

Cullity BD, Stock SR (2001) Elements of X-ray diffraction. Prentice-Hall, Inc., Upper Saddle River

Hench LL (1997) Sol–gel materials for bioceramic applications. Curr Opin Solid 2:604–610

Hench LL, Polak JM (2002) Third-generation biomedical materials. Science 295:1014–1017

Hench LL, Splinter RJ, Allen WC, Greenlee TK (1971) Bonding mechanisms at the interface of ceramic prosthetic materials. J Biomed Mater Res 5:117–141

KuKubo T, Ito S, Huang ZT, Hayashi T, Sakka S, Kitsugi T, Yamamuro T (1990) Ca, P-rich layer formed on high strength bioactive glass–ceramic A-W. J Biomed Mater Res 24:331–343

Li R, Clark AE, Hench LL (1991) An investigation of bioactive glass powders by sol–gel processing. J Appl Biomater 2:231–239

Mačković M, Hoppe A, Detsch R, Mohn D, Stark WJ, Spiecker E, Boccaccini AR (2012) Bioactive glass (type 45S5) nanoparticles: in vitro reactivity on nanoscale and biocompatibility. J Nanopart Res 14. doi:10.1007/s11051-012-0966-6

Messing GL, Zhang SC, Jayanthi GV (1993) Ceramic powder synthesis by spray-pyrolysis. J Am Ceram Soc 76:2707–2726

Shih SJ, Chang LYS, Chen CY, Borisenko KB, Cockayne DJH (2009) Nanoscale yttrium distribution in yttrium-doped ceria powder. J Nanopart Res 11:2145–2152

Shih CJ, Chen HT, Huang LF, Lu PS, Chang HF, Chang IL (2010) Synthesis and in vitro bioactivity of mesoporous bioactive glass scaffolds. Mater Sci Eng C 30:657–663

Shih SJ, Wu YY, Borisenko KB (2011) Control of morphology and dopant distribution in yttrium-doped ceria nanoparticles. J Nanopart Res 13:7021–7028

Shih SJ, Wu YY, Chen CY, Yu CY (2012) Morphology and formation mechanism of ceria nanoparticles by spray pyrolysis. J Nanopart Res 14:1–9

Song YL, Tsai SC, Chen CY, Tseng TK, Tsai CS, Chen JW, Yao YD (2004) Ultrasonic spray pyrolysis for synthesis of spherical zirconia particles. J Am Ceram Soc 87:1864–1871

Vallet-Regi M (2001) Ceramics for medical applications. J Chem Soc 97–108

Vallet-Regi M, Balas F, Colilla M, Manzano M (2008) Bone-regenerative bioceramic implants with drug and protein controlled delivery capability. Prog Solid State Chem 36:163–191

Vogel W, Höland W (1982) Nucleation and crystallization kinetics of an $MgO–Al_2O_3–SiO_2$ base glass when using different doping agents. Z Chem 22:429–438

Vogel W, Höland W, Naumann K, Gummel J (1986) Development of machineable bioactive glass ceramics for medical uses. J Non-Cryst Solids 80:34–51

Xia W, Chang J (2006) Well-ordered mesoporous bioactive glasses (MBG): a promising bioactive drug delivery system. J Control Release 110:522–530

Xia W, Chang J (2008) Preparation, in vitro bioactivity and drug release property of well-ordered mesoporous 58S bioactive glass. J Non-Cryst Solids 354:1338–1341